IEEE Photonics Journal
An IEEE Photonics Society Publication

Open Access

Theoretical Study on Novel and Efficient Near-Infrared Multiphoton Quantum Splitting in Ho^{3+} Ion-Doped β-$NaYF_4$ Phosphor for Solar Energy Conversion

Volume 5, Number 2, April 2013

Pei Song
Chun Jiang

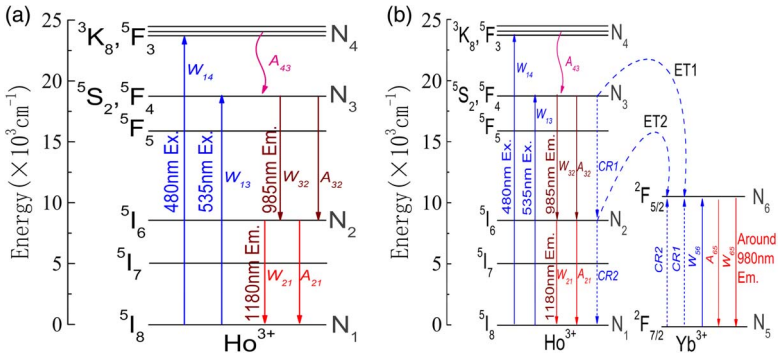

DOI: 10.1109/JPHOT.2013.2249503
1943-0655/$31.00 ©2013 IEEE

Theoretical Study on Novel and Efficient Near-Infrared Multiphoton Quantum Splitting in Ho^{3+} Ion-Doped β-$NaYF_4$ Phosphor for Solar Energy Conversion

Pei Song and Chun Jiang

State Key Laboratory of Advanced Optical Communication Systems and Networks, Shanghai Jiao Tong University, Shanghai 200240, China

DOI: 10.1109/JPHOT.2013.2249503
1943-0655/$31.00 ©2013 IEEE

Manuscript received January 10, 2013; revised February 18, 2013; accepted February 20, 2013. Date of publication March 7, 2013; date of current version March 12, 2013. This work was supported in part by the National Natural Science Foundation of China under Grant 61177056 and in part by the Shanghai Pujiang Program. Corresponding author: C. Jiang (e-mail: cjiang@sjtu.edu.cn).

Abstract: A novel application of near-infrared quantum splitting (NIR QS) that splits one ultraviolet-visible photon into NIR multiphotons can be developed for solar energy conversion. In this paper, we theoretically investigate the underlying mechanism of NIR QS in Ho^{3+} single- and Ho^{3+}–Yb^{3+} dual-doped β-$NaYF_4$ by modeling and solving rate and power propagation equation system. The highest quantum efficiency is estimated to be 257% among studied systems. The total amount of output NIR photons may be increased to meet the purpose of potentially enabling a Si-cell with a photoelectric conversion efficiency enhancement. This paper could benefit for further exploring a promising NIR QS system in the exciting field of photonic devices and materials.

Index Terms: Near-infrared quantum splitting (NIR QS), downconversion (DC), Holmium rare-earth (RE) material, $NaYF_4$ phosphor, solar cell, theoretical model.

1. Introduction

The main energy loss in the single-junction Si-cell for converting solar energy to electricity is related to the mismatch between the solar spectrum and the band-gap energy of Si-cells. Particularly, the incident solar spectrum exhibits its maximum at around 550 nm and strong contributions from ultraviolet (UV) to the blue spectral region of relatively high photon energy. For photons with energy lower than the band gap, the energy cannot be absorbed, whereas for photons with energy larger than the band gap, the excess energy is lost by thermalization of hot charge carriers. The spectral mismatch limits energy conversion efficiency of Si-cells [1]. It is obvious that one problem still to be solved is how to modify the incident solar spectrum to fit well with the Si-cells' spectral response. The solar spectral converting entities convert the wavelengths where the spectral response is low to wavelengths where the spectral response is high, consequently, using photoluminescent converting materials to modify the incident solar spectrum, particularly on the high photon energy side, is therefore significant [2]–[5]. Near-infrared (NIR) multiphoton quantum splitting (QS) has been first achieved in the vacuum UV spectral region of Pr^{3+}-doped fluorides [6]–[8]. If one UV-visible photon can be split into NIR multiphotons, a novel application for NIR multiphoton QS will be developed in the exciting field of solar energy conversion. Downconversion (DC) phenomena have been investigated in many systems, such as RE^{3+}–Yb^{3+} (RE = Yb, Tm, Ce, Nd, and Pr) couples [9]–[12],

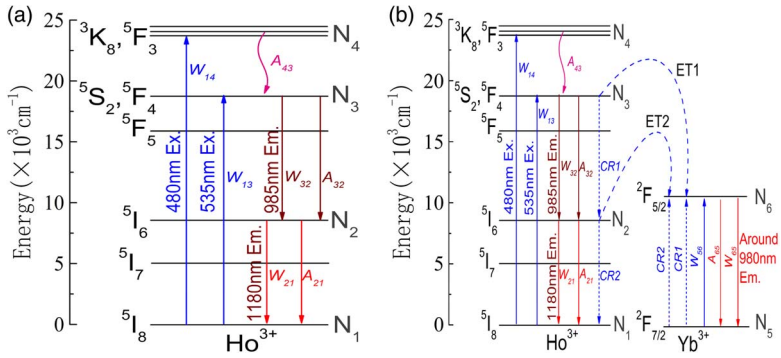

Fig. 1. (a) Energy level scheme and NIR two-photon QS mechanism in Ho^{3+} single-doped β-$NaYF_4$ system. (b) Energy level scheme and NIR two-photon QS mechanism in Ho^{3+}–Yb^{3+} dual-doped β-$NaYF_4$ system, showing ET and DC processes.

however, in most of those systems where NIR luminescence originates from Yb^{3+} ion through a first-order energy transfer (ET) from RE^{3+} rather than a QS process. It seems that there are presently few related studies on NIR multiphoton QS, particularly NIR three-photon QS, and thus, the main mechanisms of NIR QS are rarely available.

Recently, some promising phenomena, including NIR multiphoton QS in Ho^{3+} single- and Ho^{3+}–Yb^{3+} dual-doped β-$NaYF_4$, have been reported in experiments [13]–[16]. While in this paper, we detailedly investigate the theoretical model system and the underlying mechanism of NIR multiphoton QS in Ho^{3+} single- and Ho^{3+}–Yb^{3+} dual-doped β-$NaYF_4$ based on the spectroscopic data.

2. Theoretical Model

The theoretical rate and power density equations models of the RE-doped system for fiber and waveguide amplifiers have been previously presented [17]–[23]. In our paper, we investigate the NIR multiphoton QS model of Ho^{3+} single- and Ho^{3+}–Yb^{3+} dual-doped β-$NaYF_4$ systems by proposing the rate and power density propagation equations. The NIR multiphoton QS system of Ho^{3+} single and Ho^{3+}–Yb^{3+} dual doped is equivalent to the system of pump-excitation-transition where the population rate equations show the NIR multiphoton QS process of the Ho^{3+} single- and Ho^{3+}–Yb^{3+} dual-doped systems and the power density propagation equations show absorption and reemission of input solar light during transmission within the layers of spectral downconverting. These theoretical models are based on experimental values from literatures and calculated in MATLAB.

2.1. NIR Two-Photon QS in Ho^{3+} Single- and Ho^{3+}–Yb^{3+} Dual-Doped β-$NaYF_4$ System

The diagram of energy levels, the relevant absorption, emission transitions, and spontaneous emission in Ho^{3+} single-doped β-$NaYF_4$ NIR two-photon QS system are shown in Fig. 1(a). When excited by blue photons into the $(^3K_8, ^5F_3)$ level under 480-nm excitation followed by fast nonradiative relaxation (NR) to the $(^5S_2, ^5F_4)$ level, the $(^5S_2, ^5F_4)$ state of Ho^{3+} ion populated by fast multiphonon relaxation can efficiently emit a 985-nm NIR photon through the $(^5S_2, ^5F_4) \rightarrow {}^5I_6$ transition (first step). Subsequently, the electrons in $^5I_6$ level induce another relaxation by emission of an 1180-nm photon (second step). When directly excited by blue photons into the $(^5S_2, ^5F_4)$ level under 535-nm excitation, the sequential two-step transitions of the second and the third occur, where the $^5I_6$ level acts as the intermediate level.

The diagram of energy levels, the relevant absorption, emission transitions, spontaneous emission, and ET process in Ho^{3+}–Yb^{3+} dual-doped β-$NaYF_4$ NIR two-photon QS system are shown in Fig. 1(b). Under excitation of 480 nm, the $(^5S_2, ^5F_4)$ state of Ho^{3+} ion populated fast by phonon-assisted NR can efficiently excite the $^2F_{5/2}$ state of Yb^{3+} to emit a 985-nm photon (first step)

through the resonant cross-relaxation (CR) process: $Ho^{3+}(^5S_2, ^5F_4) + Yb^{3+}(^2F_{7/2}) \rightarrow Ho^{3+}(^5I_6) + Yb^{3+}(^2F_{5/2})$ (CR1). Subsequently, the electrons in the $^5I_6$ level induce another resonant CR process that yields a 985-nm photon (second step): $Ho^{3+}(^5I_6) + Yb^{3+}(^2F_{7/2}) \rightarrow Ho^{3+}(^5I_8) + Yb^{3+}(^2F^{5/2})$ (CR2), due to their nearly equivalent energy gaps 10 000 cm^{-1}.

A group of rate equations (1), (3), (5), and (7) and power density propagation equations (10) and (12) are made up of Ho^{3+} single-doped β-$NaYF_4$ NIR two-photon QS system and a group of equations (2), (4), (6), (7)–(9), (11), and (13) are made up of Ho^{3+}–Yb^{3+} dual-doped β-$NaYF_4$ NIR two-photon QS system as follows:

$$\frac{\partial N_1}{\partial t} = W_{21}N_2 + A_{21}N_2 - W_{14}N_1 - W_{13}N_1 \tag{1}$$

$$\frac{\partial N_1}{\partial t} = W_{21}N_2 + A_{21}N_2 - W_{14}N_1 - W_{13}N_1 + C_{cr2}N_2N_5 \tag{2}$$

$$\frac{\partial N_2}{\partial t} = W_{32}N_3 + A_{32}N_3 - W_{21}N_2 - A_{21}N_2 \tag{3}$$

$$\frac{\partial N_2}{\partial t} = W_{32}N_3 + A_{32}N_3 - W_{21}N_2 - A_{21}N_2 + C_{cr1}N_3N_5 - C_{cr2}N_2N_5 \tag{4}$$

$$\frac{\partial N_3}{\partial t} = A_{43}N_4 + W_{13}N_1 - W_{32}N_3 - A_{32}N_3 \tag{5}$$

$$\frac{\partial N_3}{\partial t} = A_{43}N_4 + W_{13}N_1 - W_{32}N_3 - A_{32}N_3 - C_{cr1}N_3N_5 \tag{6}$$

$$\frac{\partial N_4}{\partial t} = W_{14}N_1 - A_{43}N_4 \tag{7}$$

$$\frac{\partial N_5}{\partial t} = W_{65}N_6 + A_{65}N_6 - W_{56}N_5 - C_{cr1}N_3N_5 - C_{cr2}N_2N_5 \tag{8}$$

$$\frac{\partial N_6}{\partial t} = W_{56}N_5 - W_{65}N_6 - A_{65}N_6 + C_{cr1}N_3N_5 + C_{cr2}N_2N_5 \tag{9}$$

$$\frac{dP_p(z,\lambda)}{dz} = [\sigma_{41}(\lambda)N_4 + \sigma_{31}(\lambda)N_3 - \sigma_{14}(\lambda)N_1 - \sigma_{13}(\lambda)N_1]P_p(z,\lambda) - \alpha_p P_p(z,\lambda) \tag{10}$$

$$\frac{dP_p(z,\lambda)}{dz} = [\sigma_{32}(\lambda)N_3 + \sigma_{21}(\lambda)N_2 - \sigma_{14}(\lambda)N_1 - \sigma_{13}(\lambda)N_1]P_p(z,\lambda) - \alpha_p P_p(z,\lambda) \tag{11}$$

$$\frac{dP_s(z,\lambda)}{dz} = [\sigma_{32}(\lambda)N_3 + \sigma_{21}(\lambda)N_2 - \sigma_{12}(\lambda)N_1 - \sigma_{23}(\lambda)N_2]P_s(z,\lambda) - \alpha_s P_s(z,\lambda) \tag{12}$$

$$\frac{dP_s(z,\lambda)}{dz} = [\sigma_{65}(\lambda)N_6 - \sigma_{56}(\lambda)N_5]P_s(z,\lambda) - \alpha_s P_s(z,\lambda) \tag{13}$$

where $N_1(^5I_8)$, $N_2(^5I_6)$, $N_3(^5S_2, ^5F_4)$, $N_4(^3K_8, ^5F_3)$, $N_5(^2F_{7/2})$, and $N_6(^2F_{5/2})$ are the population densities of relevant energy levels of Ho^{3+} and Yb^{3+}, and N_i $(i, j = 1\text{–}6)$ is dependent of the thickness of doping layer z. A_{ij} $(i, j = 1\text{–}6)$ are the respective spontaneous transition rates and nonradiation transition rates between energy levels i and j. $\sigma_{ij}(\lambda)$ $(i, j = 1\text{–}6)$ is the absorption and emission cross section of the transition between the energy levels i and j. $P_p(z,\lambda)$ and $P_s(z,\lambda)$ are the corresponding input solar power density and output light power density. α_p and α_s are the scattering loss and are assumed as a frequency-independent constant for simplification. C_{cr1} and C_{cr2} are the ET coefficient describing processes of CR1 and CR2 and are linearly increasing functions of Ho^{3+} ion concentrations according to the theory of the resonant ET [24], i.e.,

$$C_{CR1} = C_{CR2} = 8.00 \times 10^{-48}(N_{Ho3+} - 1.0 \times 10^{25}) + 2.0 \times 10^{-21} \tag{14}$$

W_{ij} $(i, j = 1\text{–}6)$ is the transition rate between energy levels i and j and can be expressed as

$$W_{ij}(z,\lambda) = \frac{\sigma_{ij}(\lambda)P(z,\lambda)}{h\nu_{ij}A_{eff}} \tag{15}$$

where h is the Planck's constant, v_{ij} is the bandwidth, and A_{eff} is the effective cross-sectional area.

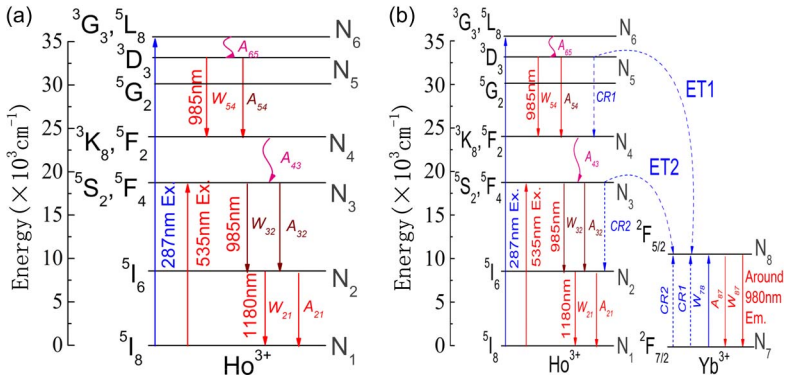

Fig. 2. (a) Energy level scheme and NIR three-photon QS mechanism in Ho^{3+} single-doped β-$NaYF_4$ system. (b) Energy level scheme and NIR three-photon QS mechanism in Ho^{3+}–Yb^{3+} dual-doped β-$NaYF_4$ system, showing ET and DC processes.

Total Ho^{3+}, Yb^{3+} concentrations N_{Ho3+} and N_{Yb3+} are assumed to be constant within the whole Ho^{3+} single- or Ho^{3+}–Yb^{3+} dual-doped β-$NaYF_4$ system that satisfy the conservation conditions

$$\sum_{i=1}^{4} N_i(z) - N_{Ho3+} = 0 \tag{16}$$

$$\sum_{i=5}^{6} N_i(z) - N_{Yb3+} = 0. \tag{17}$$

2.2. NIR Three-Photon QS in Ho^{3+} Single- and Ho^{3+}/Yb^{3+} Dual-Doped β-$NaYF_4$ System

The schematic energy level diagram of Ho^{3+} single-doped β-$NaYF_4$ system depicts the sequential NIR three-photon QS process, as shown in Fig. 2(a). When excited by blue photons into the $(^3G_3, ^5L_8)$ level under the 287-nm excitation followed by fast NR to the $^3D_3$ level, the $^3D_3$ state of Ho^{3+} ion populated by fast multiphonon relaxation can efficiently emit a 985-nm NIR photon through the $^3D_3 \rightarrow (^3K_8, ^5F_2)$ transition (first step). The excited $^3D_3$ state of Ho^{3+} is the long-lived level because of the large energy gap of $^3D_3 \rightarrow {}^5G_2$ (around 2800 cm^{-1}) but small maximum phonon energy of $NaYF_4$ host lattice (around 400 cm^{-1}). Following the $(^5S_2, ^5F_4)$ states populated by the phonon-assisted NR from the excited $(^3K_8, ^5F_2)$ states, relaxation to the $^5I_6$ level radiatively occurs by emission of a 985-nm photon (second step). Finally, the $^5I_6$ level relaxes by emission of an 1180-nm photon (third step), completing a process of NIR three-photon QS. When directly excited by blue photons into the $(^5S_2, ^5F_4)$ level under 535-nm excitation, the sequential two-step transitions of the second and the third occur, where the $^5I_6$ level acts as the intermediate level. The typical energy gaps of around 2900 and 3500 cm^{-1} enable radiative decay to dominate over multiphonon relaxation of the $(^5S_2, ^5F_4)$ and $^5I_6$ states. Hence, these levels serve as intermediate levels of the NIR three-photon QS process.

The schematic energy level diagram of the Ho^{3+}–Yb^{3+} dual-doped β-$NaYF_4$ system depicts the sequential NIR three-photon QS, ET, and DC processes, as shown in Fig. 2(b). Under excitation of 287 nm, the $^3D_3$ state of Ho^{3+} ion populated fast by phonon-assisted NR can efficiently excite the $^2F_{5/2}$ state of Yb^{3+} to emit a 985-nm photon (first step) through the resonant CR process: $Ho^{3+}(^3D_3) + Yb^{3+}(^2F_{7/2}) \rightarrow Ho^{3+}(^3K_8, ^5F_2) + Yb^{3+}(^2F_{5/2})$ (CR1). Following the $(^5S_2, ^5F_4)$ states nonradiatively populated from the excited $(^3K_8, ^5F_2)$ states, the resonant ET could effectively occur to yield a 985-nm photon (second step): $Ho^{3+}(^5S_2, ^5F_4) + Yb^{3+}(^2F_{7/2}) \rightarrow Ho^{3+}(^5I_6) + Yb^{3+}(^2F_{5/2})$ (CR2) due to their nearly equivalent energy gaps 10 000 cm^{-1}. Another 1180-nm NIR photon emission can be sequentially induced by Ho^{3+} spontaneous (third step): $Ho^{3+}(^5I_6) \rightarrow Ho^{3+}(^5I_8)$.

When under the 535-nm excitation, the sequential two-step transitions of the second and the third occur.

A group of rate equations (18), (19), (21), (23), (25), and (27), shown below, and power density propagation equations (30) and (32), shown below, are made up of Ho^{3+} single-doped β-$NaYF_4$ NIR three-photon QS system and a group of equations (18), (20), (22), (24), (26), (28), (29), (31), and (33), shown below, are made up of Ho^{3+}–Yb^{3+} dual-doped β-$NaYF_4$ NIR three-photon QS system as follows:

$$\frac{\partial N_1}{\partial t} = W_{21}N_2 + A_{21}N_2 - W_{16}N_1 - W_{13}N_1 \tag{18}$$

$$\frac{\partial N_2}{\partial t} = W_{32}N_3 + A_{32}N_3 - W_{21}N_2 - A_{21}N_2 \tag{19}$$

$$\frac{\partial N_2}{\partial t} = W_{32}N_3 + A_{32}N_3 - W_{21}N_2 - A_{21}N_2 + C_{CR2}N_3N_7 \tag{20}$$

$$\frac{\partial N_3}{\partial t} = A_{43}N_4 - W_{32}N_3 - A_{32}N_3 + W_{13}N_3 \tag{21}$$

$$\frac{\partial N_3}{\partial t} = A_{43}N_4 - W_{32}N_3 - A_{32}N_3 + W_{13}N_3 - C_{CR2}N_3N_7 \tag{22}$$

$$\frac{\partial N_4}{\partial t} = W_{54}N_5 + A_{54}N_5 - W_{43}N_4 \tag{23}$$

$$\frac{\partial N_4}{\partial t} = W_{54}N_5 + A_{54}N_5 - W_{43}N_4 + C_{CR1}N_5N_7 \tag{24}$$

$$\frac{\partial N_5}{\partial t} = A_{65}N_6 - W_{54}N_5 - A_{54}N_5 \tag{25}$$

$$\frac{\partial N_5}{\partial t} = A_{65}N_6 - W_{54}N_5 - A_{54}N_5 - C_{CR1}N_5N_7 \tag{26}$$

$$\frac{\partial N_6}{\partial t} = W_{16}N_1 - A_{65}N_6 \tag{27}$$

$$\frac{\partial N_7}{\partial t} = W_{87}N_8 + A_{87}N_8 - W_{78}N_7 - C_{CR2}N_3N_7 - C_{CR1}N_5N_7 \tag{28}$$

$$\frac{\partial N_8}{\partial t} = W_{78}N_7 - W_{87}N_8 - A_{87}N_8 + C_{CR1}N_5N_7 + C_{CR2}N_3N_7 \tag{29}$$

$$\frac{dP_p(z,\lambda)}{dz} = [\sigma_{61}(\lambda)N_6 + \sigma_{31}(\lambda)N_3 - \sigma_{16}(\lambda)N_1 - \sigma_{13}(\lambda)N_1]P_{p1}(z,\lambda) - \alpha_p P_p(z,\lambda) \tag{30}$$

$$\frac{dP_p(z,\lambda)}{dz} = [\sigma_{54}(\lambda)N_5 + \sigma_{32}(\lambda)N_3 + \sigma_{21}(\lambda)N_2 - \sigma_{16}(\lambda)N_1]P_{p1}(z,\lambda) - \alpha_p P_p(z,\lambda) \tag{31}$$

$$\frac{dP_s(z,\lambda)}{dz} = [\sigma_{54}(\lambda)N_5 + \sigma_{32}(\lambda)N_3 + \sigma_{21}(\lambda)N_2 - \sigma_{12}(\lambda)N_1 - \sigma_{23}(\lambda)N_2 - \sigma_{45}(\lambda)N_4]P_s(z,\lambda) - \alpha_s P_s(z,\lambda) \tag{32}$$

$$\frac{dP_s(z,\lambda)}{dz} = [\sigma_{87}(\lambda)N_8 - \sigma_{78}(\lambda)N_7]P_s(z,\lambda) - \alpha_s P_s(z,\lambda) \tag{33}$$

where $N_1(^5I_8)$, $N_2(^5I_6)$, $N_3(^5S_2, ^5F_4)$, $N_4(^3K_8, ^5F_2)$, $N_5(^3D_8)$, $N_6(^3G_3, ^5L_8)N_7(^2F_{7/2})$, and $N_8(^2F_{5/2})$ are the population densities of relevant energy levels of Ho^{3+} and Yb^{3+}. N_i $(i = 1–8)$, A_{ij} $(i,j = 1–8)$, $\sigma_{ij}(\lambda)$ $(i,j = 1–8)$, $P_p(z,\lambda)$, $P_s(z,\lambda)$, α_p, α_s, C_{CR1}, C_{CR2}, W_{ij} $(i,j = 1–8)$, and the satisfied conservation conditions of total Ho^{3+}, Yb^{3+} concentrations N_{Ho3+}, N_{Yb3+} are consistent with pervious definitions.

2.3. System Modeling

For calculating NIR multiphoton QS systems in Ho^{3+} single- and Ho^{3+}–Yb^{3+} dual-doped β-$NaYF_4$, we consider an initial time-independent steady-state $\partial n_i/\partial t = 0$ and can numerically

TABLE 1
Spectroscopic parameters for NIR multiphoton QS in Ho^{3+} single- and Ho^{3+}–Yb^{3+} dual-doped β-$NaYF_4$

Parameter (Symbol)	Value (Unit)
Scattering loss coefficient (α_p)	0.1 (db/m)
Scattering loss coefficient (α_s)	0.1 (db/m)
Ho^{3+} 287 nm absorption cross section (σ_{16}) #	5.74×10^{-22} (m^2)
Ho^{3+} 480 nm absorption cross section (σ_{14})	1.61×10^{-22} (m^2)
Ho^{3+} 535 nm absorption cross section (σ_{13})	7.31×10^{-22} (m^2)
Ho^{3+} 985 nm radiation cross section (σ_{32})	1.63×10^{-22} (m^2)
Ho^{3+} 985 nm radiation cross section (σ_{54}) ##	1.71×10^{-22} (m^2)
Ho^{3+} 1180 nm radiation cross section (σ_{21})	3.21×10^{-22} (m^2)
Ho^{3+} spontaneous emission rate (A_{32})	2325.41 (s^{-1})
Ho^{3+} spontaneous emission rate (A_{21})	253.38 (s^{-1})
Ho^{3+} spontaneous emission rate (A_{65}) ##	935.32 (s^{-1})
Ho^{3+} spontaneous emission rate (A_{54}) ##	389.13 (s^{-1})
Ho^{3+} spontaneous emission rate (A_{43}) ##	165.32 (s^{-1})
Ho^{3+} spontaneous emission rate (A_{43}) #	560 (s^{-1})
Yb^{3+} 980 nm absorption cross section (σ_{56}) #	1.32×10^{-24} (m^2)
Yb^{3+} 980 nm absorption cross section (σ_{78}) ##	1.32×10^{-24} (m^2)
Yb^{3+} 980 nm radiation cross section (σ_{65}) #	1.40×10^{-24} (m^2)
Yb^{3+} 980 nm radiation cross section (σ_{87}) ##	1.40×10^{-24} (m^2)
Yb^{3+} spontaneous emission rate (A_{65}) #	15000 (s^{-1})
Yb^{3+} spontaneous emission rate (A_{87}) ##	15000 (s^{-1})
Initial effective input power density (P_{p01}^*)	0.175 (W/m^2)
Initial effective input power density (P_{p02}^*)	0.540 (W/m^2)
Initial effective input power density (P_{p03}^*)	0.494 (W/m^2)
Initial output power density (P_{s0})	0.540 (W/m^2)

#and ##especially refers to NIR two-photon and three-photon QS system, respectively.

solve the population rate equations by virtue of Newton's iterative method. The power density propagation equations form a system of coupled differential equations that can be numerically solved by means of fourth-order Runge–Kutta methods with boundary conditions, i.e., $P_{pi}\ (z=0,\lambda)=P_{p0i}^*\ (i=1\text{–}3)$ and $P_s(z=0,\lambda)=P_{s0}$. The spectroscopic parameters [13]–[16] used in calculation are listed in Table 1.

We choose 287, 480, and 535 nm as the center excitation wavelength of the Ho^{3+} ion and 980 nm as the center radiation wavelength of the Yb^{3+} ion, respectively. For accurately calculating the effective absorption of the input solar spectrum in the system, the Ho^{3+} excitation linewidth at around 287, 480, and 535 nm should be taken into account. Incident solar spectrum is normalized for the case of complete absorption of incident solar emission in the spectral region corresponding to the 287-, 480-, and 535-nm excitation bands of the Ho^{3+} ion. The overlap coefficient $\Gamma_i(\lambda)(i=1\text{–}3)$ of the Ho^{3+} excitation spectrum and the incident solar spectrum is defined as

$$\Gamma_i(\lambda)=\frac{\int\limits_{\lambda} I_{Ex.}^{i}(\lambda)d\lambda}{\int\limits_{\lambda} I_{So.}(\lambda)d\lambda} \tag{34}$$

where $I_{Ex.}^{i}(\lambda)(i=1\text{–}3)$ are the Ho^{3+} excitation peaks near the 287-, 480-, and 535-nm center excitation wavelength, respectively, and $I_{So.}(\lambda)$ is the solar spectrum in the 250- to 600-nm range.

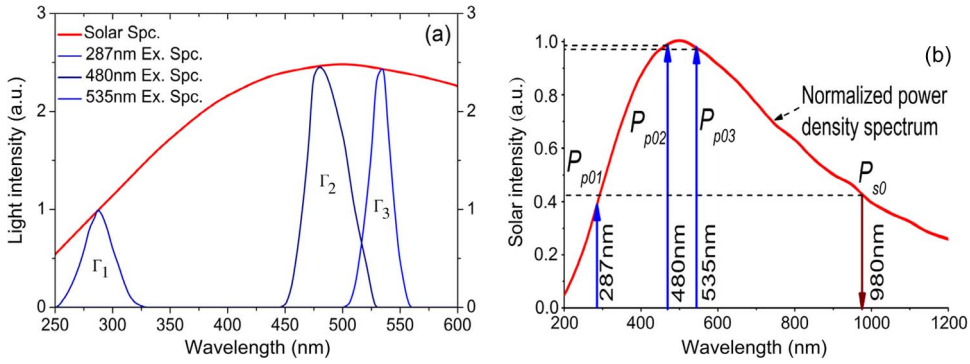

Fig. 3. (a) Ho^{3+} excitation spectrum and incident solar spectrum for calculation of $\Gamma_i(\lambda)$. (b) Normalized power density spectrum for calculation of the relation $P_{p01} : P_{p02} : P_{p03} : P_{s0} = 0.39 : 0.98 : 0.94 : 0.42$.

$\Gamma_1(\lambda)$, $\Gamma_2(\lambda)$, and $\Gamma_3(\lambda)$ are calculated as 35%, 43%, and 41%, which means such proportion of incident solar energy can be effectively absorbed in the NIR QS system, as shown in Fig. 3(a). For simulating, we set $P_{p10} = 500$ mW/m^2 as the initial input power density incident at 287 nm. Employing the spectrum of normalized solar power density [25], the initial effective input power density P^*_{p10} of 175 W/m^2, the P^*_{p20} of 540.3 W/m^2 incident at 480 nm, the P^*_{p30} of 494.1 W/m^2 incident at 535 nm, and the initial output power density P_{s0} of 540 W/m^2 are calculated by $\Gamma_1 P_{p10}$, $2.51\Gamma_2 P_{p10}$, $2.41\Gamma_3 P_{p10}$, and $1.08 P_{p10}$, respectively, as shown in Fig. 3(b). Initial N_{Ho3+}, N_{Yb3+}, and z are set to be 1.0×10^{25}, 1.0×10^{25} ions/m^3, and 5.0×10^{-3} m, respectively. The effective absorption of input solar spectrum in the NIR QS system we analyzed above is taken into account in MATLAB simulation. Finally, we obtain the power density $P(\lambda)$ of each system and can acquire the corresponding photon flux density $N(\lambda)$ by using the following relation:

$$N(z,\lambda) = \frac{P(z,\lambda)}{hc} \times 10^{-9} (\mathrm{W \cdot m^{-2} \cdot s^{-1}}) \tag{35}$$

where h is the Planck's constant, and c is the velocity of light in a vacuum.

For evaluating the effect of solar spectrum DC, we define the total QE (η) of the NIR multiphoton QS model of Ho^{3+} single- and Ho^{3+}–Yb^{3+} dual-doped β-$NaYF_4$ systems

$$\eta(z,\lambda) = \frac{\int_{\lambda=200}^{1500} N_{\mathrm{out}}(z,\lambda)d\lambda}{\int_{\lambda=200}^{1500} N_{\mathrm{in}}(z,\lambda)d\lambda} = \frac{\int_{\lambda=200}^{1500} [N_{\mathrm{in}}(z,\lambda) + N_s(z,\lambda) - N_{ab}(z,\lambda)]d\lambda}{\int_{\lambda=200}^{1500} N_{\mathrm{in}}(z,\lambda)d\lambda} \tag{36}$$

where $N_{\mathrm{out}}(\lambda)$ is the output spectrum of the total photon flux density, respectively. $N_{\mathrm{in}}(\lambda)$ is the input spectrum of photon flux density; $N_{ab}(\lambda)$ is the absorption spectrum of the Ho^{3+} photon flux density at 287, 480, and 535 nm; and $N_s(\lambda)$ is the output spectrum of Yb^{3+} photon flux density at around 980 nm, respectively.

2.4. Results and Discussion

$N_{\mathrm{out}}(\lambda)$ are shown in Fig. 4. For the Ho^{3+}–Yb^{3+} dual-doped system, it can be found that the obvious absorption peak at around 287 and 535 nm and 480 and 535 nm in the two- and three-photon QS mechanisms, respectively, and the emission peak at around 980 nm is both observed in these multiphoton QS mechanisms. Fig. 4 directly indicates the effective ET and DC processes. We can further find that the peak value of the 980-nm emission band is nearly two times as great as that of the 278- and 535-nm absorption bands and three times as great as that of the 480- and 535-nm absorption bands, respectively, which illustrate that one UV photon is split into two or three NIR photons, as correspondingly shown in Fig. 4(a) and (b). Fig. 4 illustrates that in virtue of the NIR QS,

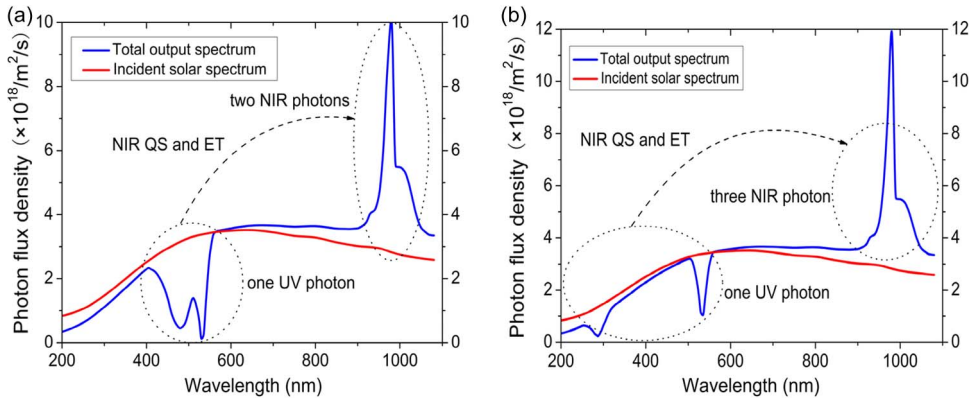

Fig. 4. (a) Modified spectrum of NIR two-photon QS in Ho^{3+} dual-doped β-$NaYF_4$ system. (b) Modified spectrum of NIR three-photon QS in Ho^{3+}–Yb^{3+} dual-doped β-$NaYF_4$ system.

TABLE 2

Theoretical valuated efficiency limit for each NIR QS system

	Ho^{3+} single-doped two-photon QS	Ho^{3+} single-doped three-photon QS	Ho^{3+}-Yb^{3+} dual-doped two-photon QS	Ho^{3+}-Yb^{3+} dual-doped three-photon QS
η (%) (in this paper)	129%	147%	178%	257%
η (%) (in literature)	110%	124%	182%	246%

the total number of output photons at around 980 nm that forms the modified solar spectrum is greatly boosted relative to the normalized solar spectrum that is directly incident at Si-cells, wherein the Si-cell may obtain more energy. Therefore, the total amount of the NIR photon output increases to meet the purpose of increasing the photovoltaic conversion efficiency of Si-cells are to be expected.

Based on the host material of β-$NaYF_4$, a variation of theoretical QE is dependent on the concentration of Ho^{3+}, Yb^{3+} ions and thickness of the ion doping layer. Through optimizing concentration and thickness in modeling, a maximum total QE in Ho^{3+}–Yb^{3+} dual-doped three-photon QS is calculated to be 257%, which is much more than 178% in Ho^{3+}–Yb^{3+} dual-doped two-photon QS, under N_{Ho3+} of 6.3×10^{25} ions/m^3, N_{Yb3+} of 1.0×10^{26} ions/m^3, and a fixed thickness of doping layer (z) of 5.0×10^{-3} m. From the aforementioned results, it is quite obvious that the total QE of the Ho^{3+} single-doped system, including the two- and three-photon QS, is enhanced by cooping Yb^{3+} ions. Based our models and analyses, we summarize theoretical efficiency limits for each system from our models and referenced documents [13]–[16] in Table 2.

3. Conclusion

In this paper, we have established an efficient and novel system for simulating the NIR multiphoton QS in the Ho^{3+} single- and Ho^{3+}–Yb^{3+} dual-doped β-$NaYF_4$. The ET and DC mechanisms of theoretical models based on the rate and power density propagation equations are studied and numerically solved by using MATLAB, and the total high QE limit of each system is acquired. The models indicate that efficient NIR QS β-$NaYF_4$: Ho^{3+}–Yb^{3+} may significantly improve the potential application in increasing the photoelectric conversion efficiency of Si-cells. Further development of an efficient NIR three-photon QS could open up a new approach toward efficient Si-cells with total QE approaches of up to 300%.

References

[1] T. Trupke, M. A. Green, and P. Würfel, "Improving solar cell efficiencies by down-conversion of high-energy photons," *J. Appl. Phys.*, vol. 92, no. 3, pp. 1668–1674, Aug. 2002.

[2] W. G. J. H. M. van Sark, "Enhancement of solar cell performance by employing planar spectral converters," *Appl. Phys. Lett.*, vol. 87, no. 15, pp. 151117-1–151117-3, Oct. 2005.

[3] W. G. J. H. M. van Sark, A. Meijerink, R. E. I. Schropp, J. A. M. van Roosmalen, and E. H. Lysen, "Enhancing solar cell efficiency by using spectral converters," *Sol. Energy Mater. Sol. Cells*, vol. 87, no. 1–4, pp. 395–409, May 2005.

[4] W. G. J. H. M. van Sark, "Simulating performance of solar cells with spectral downshifting layers," *Thin Solid Films*, vol. 516, no. 20, pp. 6808–6812, Aug. 2008.

[5] W. G. J. H. M. van Sark, A. Meijerink, R. E. I. Schropp, J. A. M. van Roosmalen, and E. H. Lysen, "Modeling improvement of spectral response of solar cells by deployment of spectral converters containing semiconductor nanocrystals," *Semiconductors*, vol. 38, no. 8, pp. 962–969, Aug. 2004.

[6] J. L. Sommerdijk, A. Bril, and A. W. de Jager, "Two photon luminescence with ultraviolet excitation of trivalent praseodymium," *J. Lumin.*, vol. 8, no. 4, pp. 341–343, Feb. 1974.

[7] W. W. Piper, J. A. de Luca, and F. D. Ham, "Cascade fluorescent decay in Pr^{3+}-doped fluorides: Achievement of a quantum yield greater than unity for emission of visible light," *J. Lumin.*, vol. 8, no. 4, pp. 344–348, Feb. 1974.

[8] R. Pappalardo, "Calculated quantum yields for photon-cascade emission (PCE) for Pr^{3+} and Tm^{3+} in fluoride hosts," *J. Lumin.*, vol. 14, no. 3, pp. 159–193, Aug. 1976.

[9] X. F. Liu, Y. Teng, Y. X. Zhuang, J. H. Xie, Y. B. Qiao, G. P. Dong, D. P. Chen, and J. R. Qiu, "Broadband conversion of visible light to near-infrared emission by Ce^{3+}, Yb^{3+}-codoped yttrium aluminum garnet," *Opt. Lett.*, vol. 34, no. 22, pp. 3565–3567, Nov. 2009.

[10] Y. Teng, J. J. Zhou, X. F. Liu, S. Ye, and J. R. Qiu, "Efficient broadband near-infrared quantum cutting for solar cells," *Opt. Exp.*, vol. 18, no. 9, pp. 9671–9676, Apr. 2010.

[11] Q. Y. Zhang, G. F. Yang, and Z. H. Jiang, "Cooperative downconversion in $GdAl_3(BO_3)_4 : RE^{3+}$, Yb^{3+} (RE = Pr, Tb, and Tm)," *Appl. Phys. Lett.*, vol. 91, no. 5, pp. 051903-1–051903-3, Jul. 2007.

[12] X. Y. Huang, D. C. Yu, and Q. Y. Zhang, "Enhanced near-infrared quantum cutting in $GdBO_3 : Tb^{3+}$, Yb^{3+} phosphors by Ce^{3+} codoping," *J. Appl. Phys.*, vol. 106, no. 11, pp. 113521-1–113521-6, Dec. 2009.

[13] D. C. Yu, X. Y. Huang, S. Ye, M. Y. Peng, Q. Y. Zhang, and L. Wondraczek, "Three-photon near-infrared quantum splitting in β-$NaYF_4 : Ho^{3+}$," *Appl. Phys. Lett.*, vol. 99, no. 16, pp. 161904-1–161904-3, Oct. 2011.

[14] D. C. Yu, S. Ye, X. Y. Huang, and Q. Y. Zhang, "Enhanced three-photon near-infrared quantum splitting in β-$NaYF_4 : Ho^{3+}$ by codoping Yb^{3+}," *AIP Adv.*, vol. 2, no. 2, pp. 022124-1–022124-7, Jun. 2012.

[15] D. C. Yu, X. Y. Huang, S. Ye, Q. Y. Zhang, and J. Wang, "A sequential two-step near-infrared quantum splitting in Ho^{3+} singly doped $NaYF_4$," *AIP Adv.*, vol. 1, no. 4, pp. 042161-1–042161-6, Dec. 2011.

[16] D. C. Yu, X. Y. Huang, S. Ye, and Q. Y. Zhang, "Efficient first-order resonant near-infrared quantum cutting in β-$NaYF_4 : Ho^{3+}$, Yb^{3+}," *J. Alloys Compd.*, vol. 509, no. 41, pp. 9919–9923, Oct. 2011.

[17] E. Yahel and A. Hardy, "Modeling high-power Er^{3+}–Yb^{3+} codoped fiber lasers," *J. Lightw. Tehnol.*, vol. 21, no. 9, pp. 2044–2052, Sep. 2003.

[18] M. Karásek, "Optimum design of Er^{3+}–Yb^{3+} codoped fibers for large-signal high-pump-power applications," *IEEE J. Quantum Electron.*, vol. 33, no. 10, pp. 1699–1705, Oct. 1997.

[19] C. Jiang, "Numerical simulation of 980 nm-LD-pumped Yb^{3+}–Er^{3+}–Tm^{3+}-codoped fiber amplifier for 1500 nm and 1600 nm bands," *Adv. OptoElectron.*, vol. 2009, pp. 278105-1–278105-8, May 2009.

[20] L. Jin, D. Ma, Y. Q. Ding, and C. Jiang, "Theoretical analysis of gain characteristics of Er^{3+}–Tm^{3+}-codoped tellurite fiber amplifier," *IEEE Photon. Technol. Lett.*, vol. 18, no. 3, pp. 460–462, Feb. 2006.

[21] W. H. Xu, Y. M. Lin, and C. Jiang, "Er^{3+}–Tm^{3+}-codoped tellurite fiber amplifiers for WDM systems: A theoretical analysis of BER and bandwidth," *IEEE J. Quantum Electron.*, vol. 45, no. 1, pp. 3–9, Jan. 2009.

[22] C. Jiang and W. B. Xu, "Theoretical model of Yb^{3+}–$Er^{3+}-Tm^{3+}$-codoped system for white light generation," *J. Display Technol.*, vol. 5, no. 8, pp. 312–318, Aug. 2009.

[23] C. Jiang, "Modeling a broadband bismuth-doped fiber amplifier," *IEEE J. Sel. Topics Quantum Electron.*, vol. 15, no. 1, pp. 79–84, Jan. 2009.

[24] M. Federighi and F. Di Pasquale, "The effect of pair-induced energy transfer on the performance of silica waveguide amplifiers with high Er^{3+}/Yb^{3+} concentration," *IEEE Photon. Technol. Lett.*, vol. 7, no. 3, pp. 303–305, Mar. 1995.

[25] B. S. Richards, "Enhancing the performance of silicon solar cells via the application of passive luminescence conversion layers," *Sol. Energy Mater. Sol. Cells*, vol. 90, no. 15, pp. 2329–2337, Sep. 2006.